

# Polychromatic Optical Bloch Oscillations

Stefano Longhi

*Dipartimento di Fisica and Istituto di Fotonica e Nanotecnologie del CNR, Politecnico di Milano, Piazza L. da Vinci 32, I-20133 Milano, Italy*

Compiled June 2, 2018

Bloch oscillations (BOs) of polychromatic beams in circularly-curved optical waveguide arrays are smeared out owing to the dependence of the BO spatial period on wavelength. Here it is shown that restoring of the self-imaging property of the array and approximate BOs over relatively broad spectral ranges can be achieved by insertion of suitable lumped phase slips uniformly applied across the array.

© 2018 Optical Society of America

OCIS codes: 130.2790, 230.3120, 230.7370, 000.1600

Photonic lattices have provided in recent years a laboratory tool to visualize optical analogues of coherent phenomena generally encountered in solid-state physics, such as Bloch oscillations (BOs) [1–4] and dynamic localization (DL) [5, 6] in lattices driven by external dc or ac fields. In waveguide arrays, a common engineering approach to realize optical BOs and DL is to tailor the local curvature of the array axis [7, 8]. DL and BOs have been observed in bent waveguide arrays with either periodically-varying or constant curvature to mimic ac or dc fields [5, 6, 9, 10]. In optics, BOs and DL enable light diffraction management, with the possibility of periodic image reconstruction [8, 11]. Such a self-imaging effect, however, is generally limited to relatively narrow spectral beams. In case of DL, destruction of self-imaging for broadband beams stems from the resonant nature of the DL condition [12]. Here, periodic self-imaging is exactly fulfilled solely for a target wavelength, whereas other spectral components experience residual diffraction. In [13], Garanovich and coworkers suggested special profiles of waveguide axis curvature that mix first and second resonances of DL, leading to approximate DL over an extremely broad spectral region. The experimental demonstration of broadband DL has been very recently reported by Szameit and collaborators [14]. In case of BOs, destruction of exact self-imaging with polychromatic beams has a different reason. Here periodic beam reconstruction is exactly attained for each spectral beam component, however the self-imaging period, given by the Bloch period  $s_B$ , turns out to be proportional to the wavelength  $\lambda$ : therefore, for a beam spectrally broadened by less than  $\sim 10\%$  around its carrier, field reconstruction is fully lost just after few BO cycles. In this Letter it is shown that polychromatic optical BOs can be approximately achieved over a broad spectral range by suitable insertion of lumped phase slips in the array, which combat the dispersion of BO period with wavelength. Let us consider light propagation in low-contrast-index one-dimensional waveguide arrays with a weakly curved axis in the  $(x, z)$  plane. In the curvilinear coordinate system  $(s, \eta)$  of Fig.1(a), where  $s$  is the arc length of the curved waveguide axis, the propagation for

the spectral field component  $\psi(\eta, s; \lambda)$  at wavelength  $\lambda$  is described by the Schrödinger-like equation

$$i\hbar \frac{\partial \psi}{\partial s} = -\frac{\hbar^2}{2n_s} \frac{\partial^2 \psi}{\partial \eta^2} + [n_s - n(\eta)]\psi + n_s \kappa(s)\eta\psi \quad (1)$$

where  $\hbar = \lambda/(2\pi)$  is the reduced wavelength,  $n_s$  is the

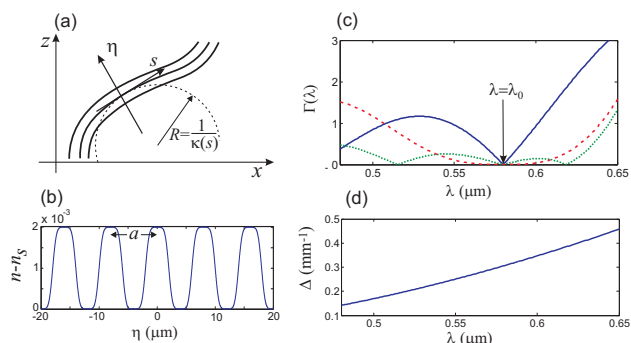


Fig. 1. (Color online) (a) Schematic of a curved waveguide array. (b) Refractive index profile  $n(\eta) - n_s$  of the array used in numerical simulations ( $a = 8 \mu\text{m}$ ,  $n_s = 1.45$ ). (c) Behavior of  $\Gamma(\lambda)$ , entering in Eq.(3), versus wavelength for (i) the 8-cm-long circularly-curved array without lumped phase slips (solid curve); (ii)  $\alpha_1 = \alpha_3 = \lambda_0/(2an_s)$  and  $\alpha_2 = 0$  (dashed curve); (iii) for  $\alpha_1 = \alpha_2 = \alpha_3 = \lambda_0/(3an_s)$  (dotted curve). (d) Behavior of waveguide coupling rate  $\Delta$  versus wavelength.

bulk refractive index,  $n(\eta)$  is the periodic index profile of the array with lattice period  $a$ , and  $\kappa(s)$  is the local curvature of waveguide axis. In the single-band and nearest-neighbor tight-binding approximations, Eq.(1) reduces to standard coupled mode equations for amplitudes  $c_n(s; \lambda)$  of modes trapped in the  $n$ -th waveguide of the array [8, 13]

$$i\dot{c}_n = -\Delta(\lambda)(c_{n+1} + c_{n-1}) + \frac{2\pi n_s \kappa(s) a n}{\lambda} c_n \quad (2)$$

where  $\Delta(\lambda)$  is the coupling rate, at wavelength  $\lambda$ , between adjacent waveguides, and the dot denotes the

derivative with respect to the arc length. Here we consider a waveguide array with constant curvature  $\kappa = 1/R$ , into which a sequence of lumped phase gradients are superimposed at the arc lengths  $s_1, s_2, \dots$ , i.e. we assume in Eq.(2)  $\kappa(s) = 1/R + \alpha_1 \delta(s-s_1) + \alpha_2 \delta(s-s_2) + \dots$ , where the parameters  $\alpha_1, \alpha_2, \dots$  define the phase slips  $\varphi_1, \varphi_2, \dots$  introduced uniformly across the array at the arc lengths  $s_1, s_2, \dots$ . The relation between the phase slip  $\varphi_l$  and the parameter  $\alpha_l$  is simply obtained after integration of Eq.(2) in the infinitesimal interval ( $s = s_l^-, s = s_l^+$ ), yielding  $\varphi_l = 2\pi n_s a \alpha_l / \lambda$ . In practice, a lumped phase gradient can be introduced (i) by a sudden tilt of waveguide axis [11] by a small angle  $\theta$ ; in this case  $\alpha_l = \theta$  and  $\varphi_l = \pi\theta/\theta_B$ , where  $\theta_B = \lambda/(2an_s)$  is the Bragg angle; (ii) by local waveguide segmentation, channel narrowing or index change modulation [15]. To investigate the self-imaging property of the arrayed structure, it is enough to consider the impulse response of the array corresponding to excitation of the waveguide  $n = 0$ . The solution to Eq.(2) with the initial condition  $c_n(0) = \delta_{n,0}$  reads [12]

$$|c_n(s)|^2 = J_n^2(2\Gamma(\lambda)), \quad (3)$$

where  $J_n$  is the Bessel function of order  $n$ ,  $\Gamma(\lambda) = \Delta(\lambda)|q(s, \lambda)|$  and

$$q(s, \lambda) = \int_0^s d\xi \exp[-i\gamma(\xi)/\lambda], \quad \gamma(s) = 2\pi n_s a \int_0^s d\xi \kappa(\xi). \quad (4)$$

The condition for self-imaging after a propagation length  $s$ , i.e.  $|c_n(s)|^2 = \delta_{n,0}$ , is thus  $q(s, \lambda) = 0$ . For the BO problem in absence of phase slips,  $\kappa(s) = 1/R$  and  $|q(s, \lambda)| = s |\sin(\pi s/s_B)| / (\pi s/s_B)$ , where

$$s_B(\lambda) = \lambda R / (n_s a) \quad (5)$$

is the BO period for the spectral field component of wavelength  $\lambda$ . For a monochromatic beam with carrier wavelength  $\lambda_0$ , periodic self-imaging is thus attained at propagation lengths  $s$  which are integer multiples of the BO cycle  $s_B(\lambda_0)$ . Unfortunately, for spectrally-broad beams different wavelength components  $\lambda$  show a shifted BO cycle  $s_B(\lambda)$ , making self-imaging and polychromatic BOs to rapidly washing out for a relatively broad spectrum of the incoming beam. As an example, Fig.2(a) shows the breakdown of self-imaging and smearing out of a breathing BO mode for polychromatic light in a  $L = 8$ -cm-long circularly-curved array as obtained by numerical simulations of Eq.(1) for an index profile of the array shown in Fig.1(b) and for a radius  $R = 40$  cm. The intensity distribution of Fig.2(a) is obtained by the incoherent superposition of five monochromatic fields of equal power (at  $\lambda = 540, 560, 580, 600$ , and  $620$  nm), which excite simultaneously the waveguide  $n = 0$ . For comparison, Fig.2(b) shows the evolution of beam intensity for the carrier spectral component solely ( $\lambda = \lambda_0 = 580$  nm), which undergoes periodic self imaging with spatial period  $s_B(\lambda_0) = \lambda_0 R / (n_s a) = 2$  cm. Note that the full propagation length  $L$  cm comprises exactly  $N = 4$  BO

cycles at the carrier wavelength. The washing out of self imaging at the output plane for a spectrally broad beam is related to the rapid deviation from zero of  $\Gamma(\lambda)$  as  $\lambda$  varies by a few percents around the reference wavelength  $\lambda_0$ , as shown by the solid curve in Fig.1(c). The allowed spectral band  $\Delta\lambda$  for (approximate) self-imaging can be roughly estimated from the condition  $2|\Gamma(\lambda)| < 1$  [see Eq.(3)], and turns out to be  $\Delta\lambda \sim 20$  nm for the solid curve of Fig.1(c). The introduction of appropriate phase slips across the array may be exploited to flatten the function  $\Gamma(\lambda)$  at around  $\lambda = \lambda_0$ . To this aim, let us consider  $(N-1)$  lumped phase gradients at  $s_1 = s_B(\lambda_0)$ ,  $s_2 = 2s_B(\lambda_0), \dots, s_{N-1} = (N-1)s_B(\lambda_0)$ , i.e. let us assume  $\kappa(s) = 1/R + \sum_{k=0}^{N-1} \alpha_k \delta(s-s_k)$  with  $s_0 = 0$  and  $\alpha_0 = 0$  for definiteness. From Eq.(4) with  $s = L$ , the expression of  $q$  can be calculated in closed form and reads

$$q(\lambda) = \frac{L}{N} \exp(-i\pi\lambda_0/\lambda) \frac{\sin(\pi\lambda_0/\lambda)}{\pi\lambda_0/\lambda} F(\pi\lambda/\lambda_0) \quad (6)$$

where we have set  $F(\xi) = \sum_{k=0}^{N-1} \exp(-2i\xi\rho_k)$  and  $\rho_k = k + (an_s/\lambda_0)(\alpha_0 + \alpha_1 + \dots + \alpha_k)$ . Appropriate choice of the values  $\alpha_k$  may flatten the shape of  $\Gamma(\lambda)$  at around its zero  $\lambda = \lambda_0$ . A first approach consists of considering the Taylor expansion of  $\Gamma(\lambda)$  at around  $\lambda_0$  and imposing  $\Gamma = (\partial\Gamma/\partial\lambda) = \dots = (\partial^M\Gamma/\partial\lambda^M) = 0$  at  $\lambda = \lambda_0$  up to a certain order  $M \geq 1$ , which defines the spectral flatness order. This requires  $F(\pi) = F'(\pi) = \dots = F^{(M-1)}(\pi) = 0$ , which yields

$$\sum_{k=0}^{N-1} \left( k + \frac{an_s}{\lambda_0} \sum_{j=0}^k \alpha_j \right)^l \exp\left(-2\pi i \frac{an_s}{\lambda_0} \sum_{j=0}^k \alpha_j\right) = 0 \quad (7)$$

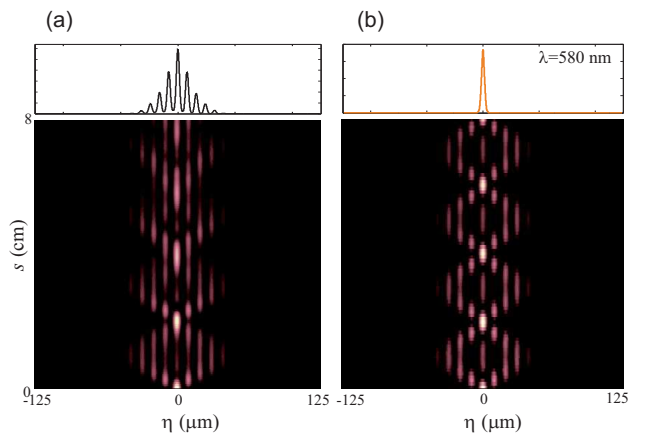


Fig. 2. (Color online) Intensity beam evolution (a) in the polychromatic, and (b) monochromatic (at carrier wavelength) regimes in a  $L = 8$ -cm-long circularly-curved array without lumped phase slips. The insets at the top are the intensity profiles at the output plane. Parameter values are given in the text.

for  $l = 0, 1, \dots, M-1$ . As an example, let us consider the case  $N = 4$ , previously discussed in Fig.2. Then one

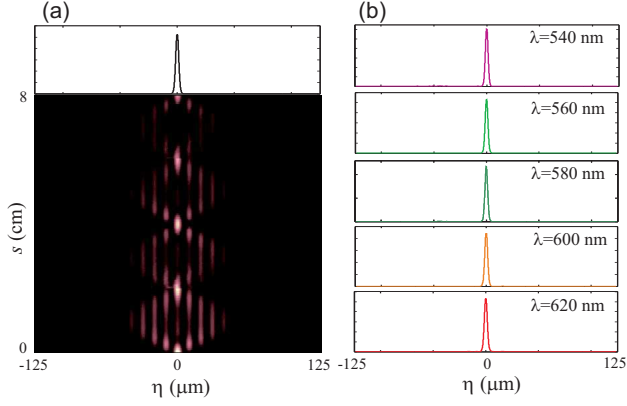


Fig. 3. (Color online) Polychromatic BOs as obtained by insertion of two lumped waveguide tilts at  $s_1 = 2$  cm and  $s_3 = 6$  cm (tilt angle  $\theta = \theta_B = 25$  mrad). In (b) the output intensity profiles at the output plane for the different spectral components are depicted.

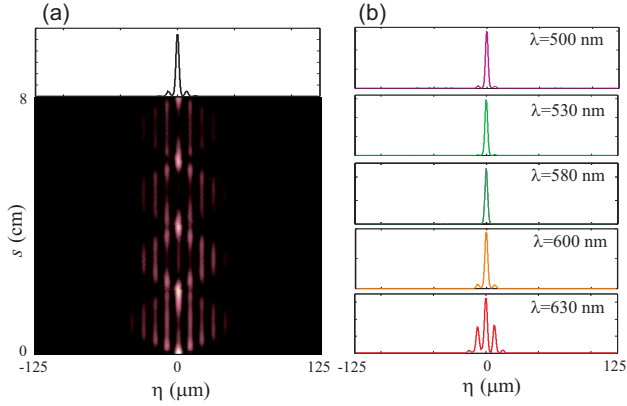


Fig. 4. (Color online) Same as Fig.3, but with the insertion of three lumped waveguide tilts at  $s_1 = 2$  cm,  $s_2 = 4$  cm and  $s_3 = 6$  cm (tilt angle  $\theta = 2\theta_B/3 \simeq 16.7$  mrad).

can check that Eq.(7) is satisfied up to the order  $M = 2$  by simply assuming  $\alpha_1 = \alpha_3 = \lambda_0/(2an_s)$  and  $\alpha_2 = 0$ . This corresponds to the introduction, at the arc lengths  $s_1 = s_B(\lambda_0)$  and  $s_3 = 3s_B(\lambda_0)$ , a lumped  $\pi$  phase shift uniformly across the array. The corresponding behavior of  $\Gamma(\lambda)$  is shown by the dashed curve in Fig.1(c). Polychromatic BOs and (approximate) self-imaging over the entire spectral range (540,620) nm is demonstrated in Fig.3(a), where the intensity evolution of the polychromatic beam of Fig.2(a) is now computed with insertion of the phase gradients at  $s_1 = s_B(\lambda_0) = 2$  cm and at  $s_3 = 3s_B(\lambda_0) = 6$  cm. In the numerical simulations, the lumped  $\pi$  phase slips are simply obtained by tilting the waveguides (tilting angle  $\theta = \theta_B = 25$  mrad) as in [11]. The spectrally-resolved output intensity profiles of the polychromatic beam are also shown in Fig.3(b). Note that, with this choice of  $\alpha_1$ ,  $\alpha_2$  and  $\alpha_3$ , the function  $\Gamma(\lambda)$  remains reasonably small in the range  $\lambda \sim (540,620)$  nm, however it rapidly increases outside this interval. A

different choice for  $\alpha_1$ ,  $\alpha_2$  and  $\alpha_3$ , which broadens the spectral range where  $2\Gamma(\lambda)$  remains smaller than  $\sim 1$ , is  $\alpha_1 = \alpha_2 = \alpha_3 = \lambda_0/(3an_s)$ . In this case,  $\Gamma'(\lambda_0)$  and  $\Gamma''(\lambda_0)$  do not vanish, however two additional zeros of  $\Gamma$  are introduced at  $\lambda \simeq 516$  nm and  $\lambda \simeq 618$  nm, as shown by the dotted curve in Fig.1(c). The corresponding behavior of polychromatic BOs, for a beam covering a spectral extent  $\Delta\lambda \simeq 130$  nm, is shown in Fig.4. Different algorithms, based on optimization methods (e.g., trying to minimize  $\int d\lambda|\Gamma(\lambda)|$ ), might be investigated to flatten the function  $\Gamma(\lambda)$  over a prescribed spectral range. As a general rule, the increase of the number  $N$  of phase gradients makes it the flattening procedure more flexible, and thus the polychromatic imaging of higher quality or applicable to a broader spectral range (for instance by increasing the spectral flattening order  $M$ ). In conclusion, broadband self-imaging based on polychromatic BOs in circularly-curved waveguide arrays has been proposed by insertion of lumped phase slips, which combat the dispersion of BO period for the various spectral beam components.

Author E-mail address: longhi@fisi.polimi.it

## References

1. R. Morandotti, U. Peschel, J. S. Aitchison, H. S. Eisenberg, and Y. Silberberg, Phys. Rev. Lett. **83**, 4756 (1999).
2. T. Pertsch, P. Dannberg, W. Elflein, A. Bräuer, and F. Lederer, Phys. Rev. Lett. **83**, 4752 (1999).
3. D.N. Christodoulides, F. Lederer, and Y. Silberberg, Nature **424**, 817 (2003).
4. R. Sapienza, P. Costantino, D. Wiersma, M. Ghulinyan, C.J. Oton, and L. Pavesi, Phys. Rev. Lett. **91**, 263902 (2003).
5. S. Longhi, M. Marangoni, M. Lobino, R. Ramponi, P. Laporta, E. Cianci, and V. Foglietti, Phys. Rev. Lett. **96**, 243901 (2006).
6. R. Iyer, J. S. Aitchison, J. Wan, M. M. Dignam, and C. M. de Sterke, Opt. Express **15**, 3212 (2007).
7. G. Lenz, I. Talanina, and M. C. de Sterke, Phys. Rev. Lett. **83**, 963 (1999).
8. S. Longhi, Opt. Lett. **30**, 2137 (2005).
9. N. Chiodo, G. DellaValle, R. Osellame, S. Longhi, G. Cerullo, R. Ramponi, P. Laporta, and U. Morgner, Opt. Lett. **31**, 1651 (2006).
10. F. Dreisow, M. Heinrich, A. Szameit, S. Döring, S. Nolte, A. Tünnermann, S. Fahr, and F. Lederer, Opt. Express **16**, 3474 (2008).
11. H. Eisenberg, Y. Silberberg, R. Morandotti, and J. Aitchison, Phys. Rev. Lett. **85**, 1863 (2000).
12. D.H. Dunlap and V.M. Kenkre, Phys. Rev. B **34**, 3625 (1986).
13. I. Garanovich, A. Sukhorukov, and Y. Kivshar, Phys. Rev. E **74**, 066609 (2006).
14. A. Szameit, I.L. Garanovich, M. Heinrich, A.A. Sukhorukov, F. Dreisow, T. Pertsch, S. Nolte, A. Tünnermann, and Y.S. Kivshar, Nature Physics **5**, 271 (2009).
15. A. Szameit, F. Dreisow, M. Heinrich, T. Pertsch, S. Nolte, A. Tünnermann, E. Suran, F. Louradour, A.

Barthélémy, and S. Longhi, Appl. Phys. Lett. **93**, 181109 (2008).